Hindawi
Shock and Vibration
Volume 2018, Article ID 1802174, 15 pages
https://doi.org/10.1155/2018/1802174

Research Article

Contact Response Analysis of Vertical Impact between Elastic Sphere and Elastic Half Space

Yang Yang, Qingliang Zeng, and Lirong Wan

Department of Mechanical and Electrical Engineering, Shandong University of Science and Technology, QingDao 266590, China

Correspondence should be addressed to Yang Yang; sdkdyangyang@126.com and Qingliang Zeng; qlzeng@sdust.edu.cn

Received 11 April 2018; Revised 14 August 2018; Accepted 27 August 2018; Published 8 November 2018

Academic Editor: Gloria Terenzi

At present, the contact problem between the particle and the plane plate is generally equivalent to the rigid sphere impacting the elastic half space or the elastic sphere impacting the rigid surface. However, in the actual contact process, there will be no rigid body, and both contact and contacted object will deform and absorb energy. The research results obtained from the equivalent of the contact material to the rigid body are less accurate. In order to obtain the accurate mechanical relation and contact response, we took the research of impact between particles and the metal plate as a breakthrough in which the particle is equivalent to an elastic sphere and the metal plate is equivalent to an elastic half space and established the theory of vertical impact contact between elastic sphere and elastic half space by the Hertz contact theory. Through the dynamic simulation of an elastic sphere which has similar properties with rock impacting target in elastic half space in LS-DYNA, the correctness of the established theory and the feasibility of the contact process simulated by LS-DYNA are verified. Based on the established theory and 3D simulation, we studied the influence law of material parameters on the contact response and analyzed the differences of the collision vibration signals caused by the different contact objects. From the above research results, we obtain that the theoretical model is more accurate to predict the maximum contact force and contact displacement in this paper than traditional Hertz theory. And the sphere radius and both contact objects' elastic modulus have larger influence on the contact response than sphere density, while the Poisson's ratio has the smallest influence on the contact response results. Different material properties will cause the different contact response. The conclusions of this paper provide a theoretical calculation method for contact and a 3D simulation method for elastic half space and provide theoretical guidance for the differences analysis of the vibration signal.

1. Introduction

In engineering applications, impact and contact problems exist everywhere. The impact of the particles on metal plate can be seen in many fields such as in the top coal mining process which is accompanied by coal or gangue impacting on the metal of the cover beam or tail beam of the caving coal hydraulic powered support, multibody systems, vehicle impact etc. The contact problem of particles impacting on the metal plate has always been a classical problem of the contact mechanism in engineering practice. At the same time, the contact between the particles and the metal plate is a complicated process, and it involves many aspects, such as the short duration of the impacts, rapid increase of transient stress, local large deformation of particle, elastoplastic properties of particle and metal plates, metal plate's flexural deflection, and other issues. At present, most theoretical research studies on the contact between particles and planes are based on the Hertz contact theory [1–6], and the particle is equivalent to spherical particles [7]. Cermik, Rossikhin, and Xie et al. studied the impact vibration response of an elastic sphere on the rigid surface with flexible balls or inflatable thin-walled balls striking the rigid target surface vertically or obliquely [8–14]. The target surface was equivalent to a rigid surface, ignoring the elastic deformation of the object being impacted. Wang et al. [15], Wang et al. [16], Willert et al. [17], Mougin et al. [18], and Jäger [19] studied the impact contact response of the rigid sphere impacting elastic plane or elastic sphere, respectively. The active plane was used as the rigid surface, and the target

plane was used as the elastic half space. They took the deformation and energy absorption of the target object into account, but they ignored the deformation and energy absorbing of the active contact object during the contact process. Wu et al. [20], Liu et al. [21], Vu-Quoc et al. [22, 23], Wang et al. [24], and Peng et al. [25] simulated and analyzed the contact process through simulation methods. Pham, Chen, Liu, and Cheng et al. investigated the effects of contact stiffness on the impact behaviour of RC beams, fracture and fragmentation responses of laminated glass under impact, ballistic performance of monolithic and multilayered steel targets penetrated by EFP, and low-velocity impact performance of scarf-repaired composite laminates [26–29]. The contact object and the target object were simultaneously equivalent to elastic materials in the simulation setup and meshed separately, and the contact response when the material under elastic-plastic deformation or the damage and destruction of the material is studied.

Based on the above research conclusions and deficiencies, in order to reveal the derivation mechanism of impact, contact response, and impact vibration law in the process of the sphere impacting the metal plate and correctly analyze the differences in vibration signals, we equated the particle to the elastic sphere and made the metal plate equivalent to the elastic half space target plate. And theoretical model of vertical impact contact between the elastic sphere and target plate in elastic half space by the Hertz contact theory is established. Meanwhile, we combined the theory with simulation by LS-DYNA to research the impact contact response between the elastic sphere and the metal plate in elastic half space and explored the influence law of material parameters on contact response. Based on the above research results, we further analyze the differences of the collision vibration signals caused by the different contact objects.

The remainder of the paper is organized as follows: Section 2 establishes the theoretical model of vertical impact contact between the elastic sphere and target plate in elastic half space. Section 3 introduces the method of constructing the simulation model of the vertical elastic impact between the elastic sphere and half space target plate and compares the analysis result of theory with simulation. Section 4 analyzes the effect of material parameters on contact response. Section 5 performs the differences analysis of vibration signals. Section 6 shows some related work and our conclusions.

2. Contact Mathematical Model of Elastic Sphere Vertically Impacting Elastic Half Space

The contact theory of elastic ball impacting rigid surface was proposed by Hertz long before. As is shown in Figure 1, Hertz theory [1–6, 30] provides the following expressions for the contact load under the condition of statics:

$$P_1 = K_1 \cdot \delta_1^{3/2}. \tag{1}$$

As is shown in Figure 2, the contact force and contact deformation of the rigid sphere contacting with elastic half space under static conditions meet the following relationship [31]:

$$P_2 = K_2 \cdot \delta_2^{3/2}. \tag{2}$$

According to the law of energy conservation, in the critical end time of compression stage,

$$\frac{1}{2}mv^2 = \int_0^{\delta_1} P_1 d\delta_1, \tag{3}$$

$$\frac{1}{2}mv^2 = \int_0^{\delta_2} P_2 d\delta_2. \tag{4}$$

From Equations (3) and (4), the maximum contact deformation and maximum contact force under two different contact conditions are obtained in the following form:

$$\delta_1 = \left(\frac{5mv^2}{4K_1}\right)^{2/5}, \tag{5}$$

$$P_1 = K_1 \cdot \left(\frac{5mv^2}{4K_1}\right)^{3/5}, \tag{6}$$

$$\delta_2 = \left(\frac{5mv^2}{4K_2}\right)^{2/5}, \tag{7}$$

$$P_2 = K_2 \cdot \left(\frac{5mv^2}{4K_2}\right)^{3/5}, \tag{8}$$

where $K_1 = 4\sqrt{R}/3 \cdot E = K$,
$K_2 = 32\sqrt{3}\sqrt{R}/27 \cdot E = 8\sqrt{3}/9 \cdot K$,
$1/E = (1-\nu_1^2/E_1) + (1-\nu_2^2/E_2)$, $1/R = (1/R_1) + (1/R_2)$, K is the Hertz contact stiffness, E_1, ν_1, E_2, and ν_2 are the elastic modulus and Poisson's ratio of the sphere (elastic or rigid) and surface (rigid surface or elastic half space), respectively, a is the contact radius, and $\delta_i\,(i = 1, 2)$ is the contact deformation.

For the problem of the elastic sphere impacting elastic half space, as is shown in Figure 3, the functional relationship of the system in the critical end time of compression stage can be expressed as

$$\begin{cases} P = P_{1t} = P_{2t} \\ \dfrac{1}{2}mv^2 = \displaystyle\int_0^{\delta_1} P_{1t}\, d\delta_{1t} + \int_0^{\delta_2} P_{2t}\, d\delta_{2t} \end{cases} \tag{9}$$

Solutions are given by

$$\delta_{1t} = \left[\frac{5mv^2}{4\left(K_1 + K_1^{5/3} \cdot K_2^{-2/3}\right)}\right]^{2/5}, \tag{10}$$

$$\delta_{2t} = \left(\frac{K_1}{K_2}\right)^{2/3} \cdot \left[\frac{5mv^2}{4\left(K_1 + K_1^{5/3} \cdot K_2^{-2/3}\right)}\right]^{2/5}, \tag{11}$$

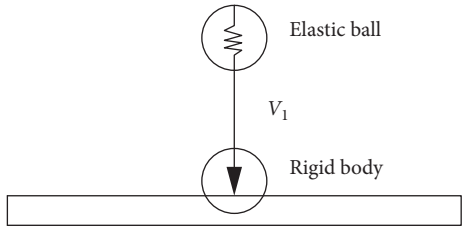

Figure 1: Elastic sphere impacting rigid surface.

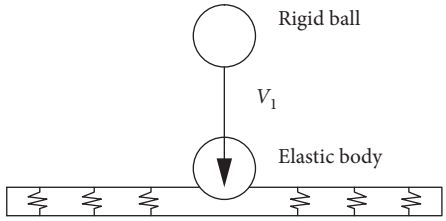

Figure 2: Rigid sphere impacting elastic half space.

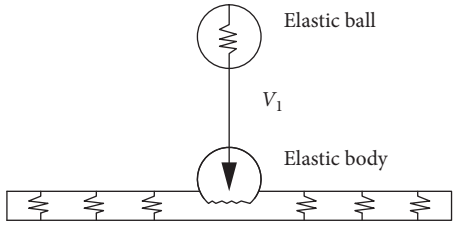

Figure 3: Elastic sphere impacting elastic half space.

$$\delta = \left[\frac{5mv^2}{4\left(K_1 + K_1^{5/3} \cdot K_2^{-2/3}\right)}\right]^{2/5} \cdot \left[1 + \left(\frac{K_1}{K_2}\right)^{2/3}\right], \tag{12}$$

$$P = K_1 \cdot \left[\frac{5mv^2}{4\left(K_1 + K_1^{5/3} \cdot K_2^{-2/3}\right)}\right]^{3/5}, \tag{13}$$

where $\delta_{it}\,(i = 1, 2)$ is the contact deformation of the elastic sphere and elastic half space, respectively, and δ is the displacement of the centre of the sphere.

For free fall impact of the elastic sphere on the metal plate, such as coal and gangue impacting the metal plate, when the rock particles such as coal or gangue is dropped from the height H in the initial vertical velocity $v_{\perp 0} = 0$ m/s, we obtain from the law of energy conservation

$$mgH = \frac{1}{2}mv_{\perp}^2 - \frac{1}{2}mv_{\perp 0}^2, \tag{14}$$

$$v_{\perp} = \sqrt{2gH}, \tag{15}$$

$$\begin{cases} \delta = \left[\frac{5mgH}{2\left(K_1 + K_1^{5/3} \cdot K_2^{-2/3}\right)}\right]^{2/5} \cdot \left[1 + \left(\frac{K_1}{K_2}\right)^{2/3}\right], \\ P = K_1 \cdot \left[\frac{5mgH}{2\left(K_1 + K_1^{5/3} \cdot K_2^{-2/3}\right)}\right]^{3/5}. \end{cases} \tag{16}$$

Select a rock material, take the material property in elastic area as the material property of the elastic sphere, and take the metal plate as target plate in elastic half space. The material parameters are shown in Table 1.

The change curves of contact displacement and contact force with different impact velocity v are obtained from Equations (5)–(8) and Equations (12)-(13), as is shown in Figures 4 and 5.

Under the ideal elastic contact condition, with the increase of impact velocity, the displacement and contact force of the rock sphere increase gradually. At the same impact speed, the displacement of centre of sphere (DCS) under condition of the elastic sphere impacting the elastic half space is biggest, the DCS under condition of the elastic sphere impacting the rigid surface is smaller, and the DCS under condition of the rigid sphere impacting the elastic half space is smallest. On the contrary, at the same impact speed, the maximum contact force under condition of rigid sphere impacting the elastic half space is biggest, the maximum contact force under condition of the elastic sphere impacting the rigid surface is smaller, and the maximum contact force under condition of the elastic sphere impacting the elastic half space is smallest. Combining Figures 4 and 5, the change curves of maximum contact force-contact displacement (MCF-CD) are obtained as shown in Figure 6. According to Equation (16), the changing curves of maximum contact force-rockfall height (MCF-RH) and contact displacement-rockfall height (CD-RH) are obtained as shown in Figure 7.

From Figure 6, with the increase of the DCS, the contact force increases exponentially. At the same DCS, the maximum contact force under condition of the rigid sphere impacting the elastic half space is biggest, the maximum contact force under condition of the elastic sphere impacting the rigid surface is smaller, and the maximum contact force under condition of the elastic sphere impacting the elastic half space is smallest. Combining Figures 4 and 5 we obtain that, the DCS calculated by the elastic sphere impacting elastic half space contact theory proposed in this paper is greater than that of the traditional theory, and the contact force is less than that of the traditional theory. Because the traditional Hertz contact theory only considers one of the contact body or the contacted body as the flexible body, the predicted contact force is too large, and the accuracy is lower when predicting the contact force by traditional theory. From Figure 7, DCS and contact force increase exponentially in the power of 2/5 and 3/5 of rockfall height, respectively.

3. Numerical Simulation of Vertical Impact Contact between Viscoelastic Sphere and Target Plate in Elastic Half Space

3.1. The Simulation Model. In this paper, we mainly studied the vertical impact contact response between the elastic sphere and target plate in elastic half space and used the finite element software LS-DYNA to establish the dynamic model of the sphere impacting the metal plates. It can be

Table 1: Parameters of contact model of the elastic sphere and metal plate.

Contact material	ρ (kg·m^{-3})	E_i (GPa)	ν	R (mm)	E (GPa)	K (N/m$^{3/2}$)
Elastic sphere	1380	2.26	0.28	25	2.4265	5.1155×10^8
Metal plate	7850	210	0.3	—		

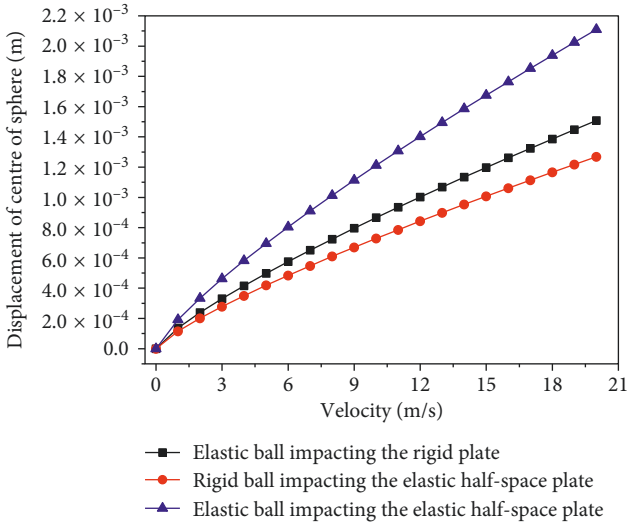

Figure 4: Displacement of centre of sphere.

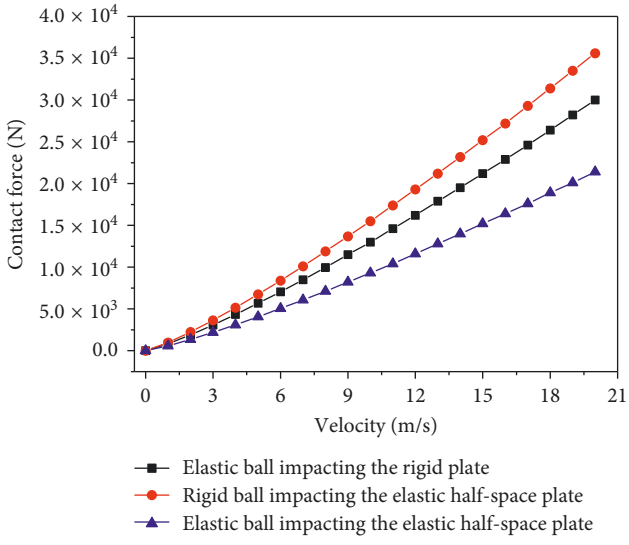

Figure 5: Maximum contact force.

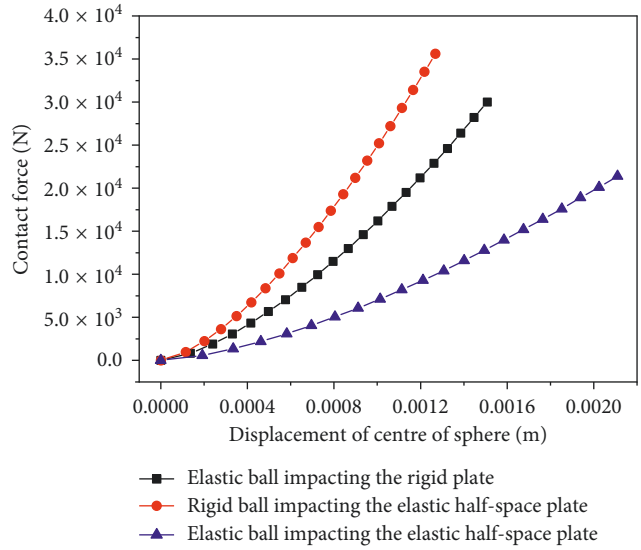

Figure 6: Curves of MCF-CD under different condition.

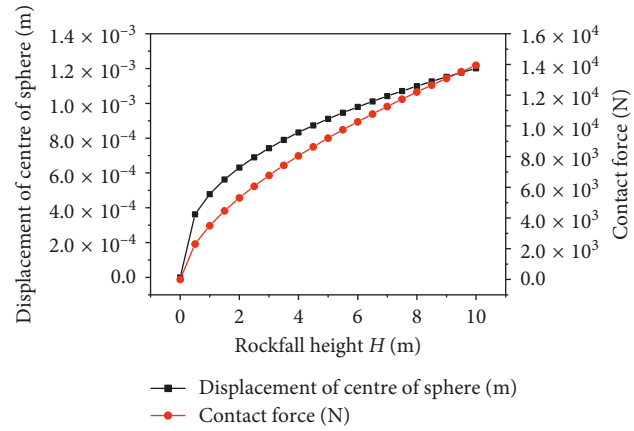

Figure 7: Curves of MCF-RH and CD-RH

seen from the Figure 8, the dynamic simulation of the single sphere with different properties impacting the metal plates vertically at different speeds was conducted. In the process of modeling, the target plate was set as the thin metal plate with homogeneous continuous medium, and the sphere models were set as the viscoelastic constitutive models with the properties of rock (coal or gangue).

In the modeling process, other factors such as air resistance were ignored. To simulate Earth's gravity, the acceleration of the sphere was defined as 9.8 m/s^2. In order to ignore the influence of the shape factor, the size R of the spheres of different attributes were all taken as 25 mm, and the simulation of 5 groups of different impact velocities such as 2 m/s, 4 m/s, 6 m/s, 8 m/s, and 10 m/s for different properties of spheres was performed. In order to prevent the sphere from overlapping with the mesh of metal plate, the gap between the end point of the sphere and the upper end-face of the metal plate was defined to be 0.000326 m, and the velocity increment of the sphere over this gap was less than 0.01 m/s, that is, less than 1/200 of the defined speed. Therefore, the effect of the gap can be negligible. To simulate the target plate in elastic half space, the boundary constraint was applied to the lower end of the metal plate after meshing the metal plate, and the constraint type was defined as full

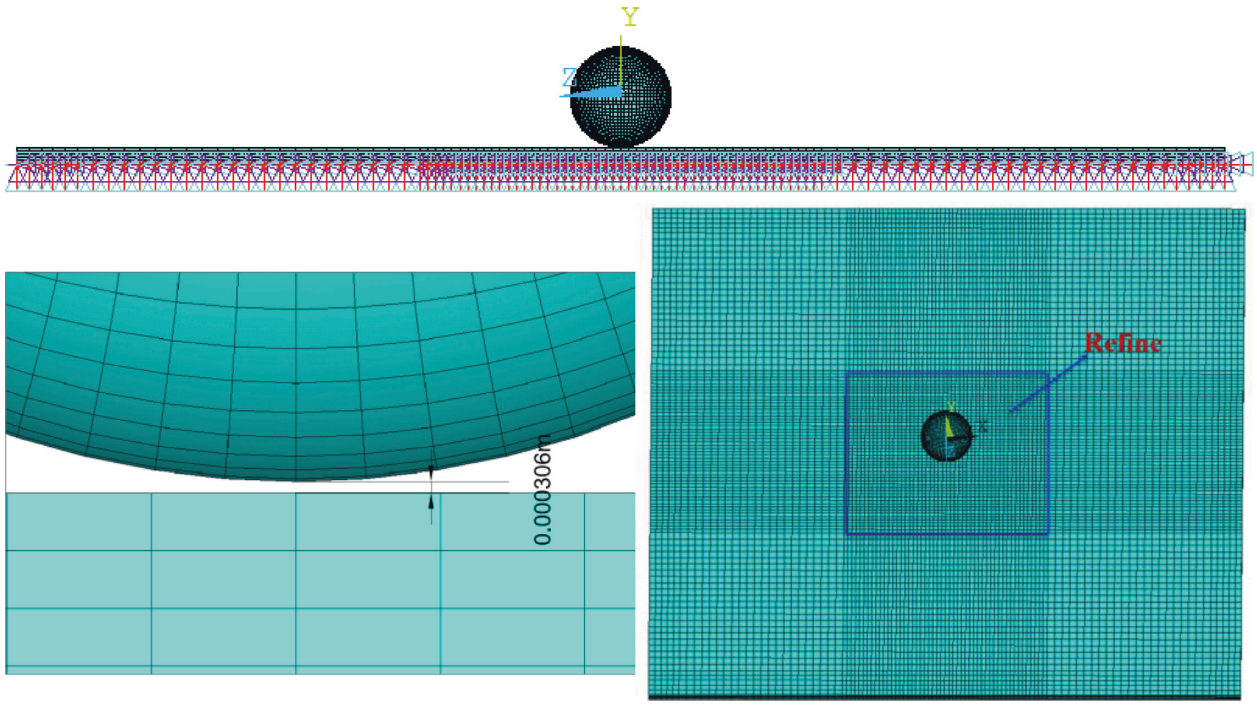

Figure 8: Simulation contact model of the elastic sphere impacting the elastic half space.

constraints. At the same time, in order to improve the quality of the simulation, hexahedral mesh is used to construct the model. The grid size of the sphere was defined as 0.002 m, and the metal plate was divided into 9 parts for meshing. The mesh of the contact areas between the sphere and the metal plate was refined. The models contain 86080 elements and 99431 nodes. Impact contact of the sphere on the metal plate is a complicated nonlinear contact. Owing to this, we set the contact type as Automatic_ Surface_ To_Surface. The surface of the sphere was set as the contact surface, and the surface of the metal plate was the target surface. The stiffness of the simulation was defined according to the contact stiffness calculated by the Hertz theory, and damping was applied during the contact process. We set the material type of the plate as elastic, and the basic material properties of the plate are similar to the $45^{\#}$ steel. The material properties of spheres and plate are shown in Table 2 ($1^{\#}$ and $2^{\#}$ elastic spheres are the elastic spheres which have the similar properties to different coal, respectively, and $3^{\#}$ and $4^{\#}$ elastic spheres are the elastic spheres which have the similar properties to different gangue, respectively.). We set the solution time as 0.001 s, each step lasts 5×10^{-7} s. To ensure the reliability of the simulation results, the hourglass energy should be less than 5% of total energy.

3.2. Comparative Analysis of Theory and Simulation Results. When the sphere with different properties impacts on the metal plates, the theoretical and simulated values of impact contact response were obtained under different impact velocities, respectively. Based on this, we got the fitting curves of the simulated values and theoretical values of the DCS, contact force, maximum contact pressure, maximum internal energy of the sphere, and the maximum internal energy of metal plate when the $1^{\#}$ sphere particle impacted on the metal plate, as shown in Figure 9. The linear correlation coefficient R^2 between the simulated values and theoretical values of the contact response of each group of materials is shown in Table 3.

From Figure 9 and Table 3, the correlation coefficient R^2 of four materials for the DCS and contact force between the simulated values and theoretical values is higher than 0.96, which shows the quite higher correlation between the simulation values and theoretical values of the DCS and contact force. The correlation coefficient R^2 for maximum internal energy of the sphere is larger than 0.85, and R^2 for maximum internal energy of the metal plate is no less than 0.84, which shows the higher correlation between the simulation values and theoretical values of the maximum internal energy of the sphere and maximum internal energy of the metal plate. Because of the large uncertainty of contact pressure, the correlation coefficient R^2 for the contact pressure is just ranging from 0.7483 to 0.85486, and there is a positive correlation between the simulated contact pressure and theoretical contact pressure. In summary, simulation results simulated by LS-DYNA have the same changing trends with the theoretical results, and the linear correlations are significant.

Figure 10 shows the variation curves of the contact force and the DCS during the initial impact and the theoretical curves of the maximum contact force and the DCS when the four types of spheres impact on the metal plate with different velocities. From the Figure 10, we can see that when the impact between the sphere and metal plate occurs, the

Table 2: Parameters of contact model of the elastic sphere and metal plate.

Material of contactant	ρ_1 (kg·m^{-3})	E_1 (GPa)	ν_1	R (mm)	E (GPa)	K (N/m$^{3/2}$)
1# elastic sphere	1380	2.26	0.28	25	2.4265	5.1155×10^8
2# elastic sphere	1550.6	4.3	0.30	25	4.6305	9.7619×10^8
3# elastic sphere	2412	21.64	0.30	25	21.559	4.5450×10^9
4# elastic sphere	2400	3.906	0.28	25	4.1618	8.7739×10^8
Material of target body	ρ_2 (kg·m^{-3})	E_2 (GPa)	ν_2	L (mm)	B (mm)	h (mm)
Metal plate	7850	210	0.30	458.4	360	8

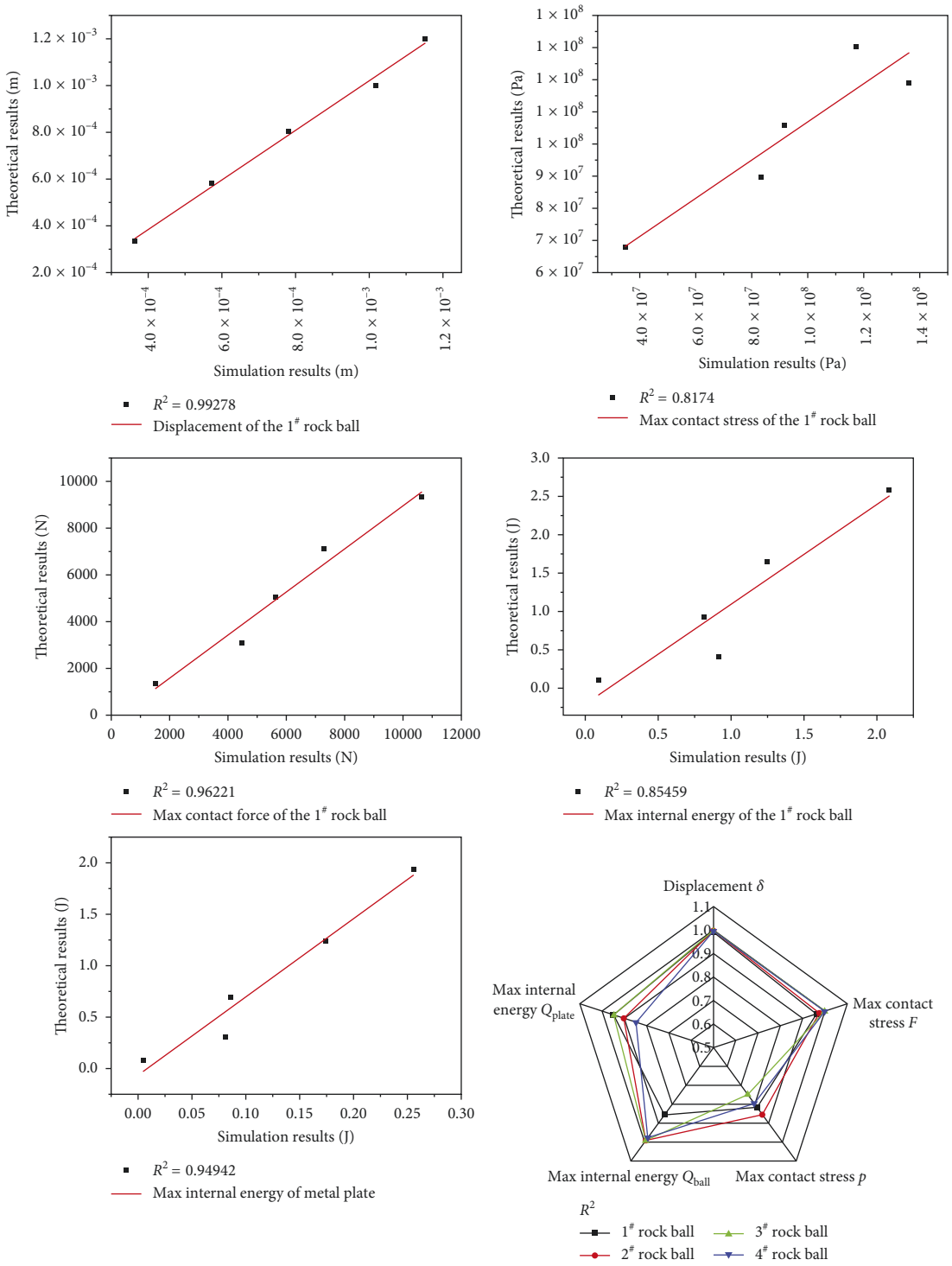

Figure 9: The relationship between the simulated values and theoretical values (take 1# material as an example).

Table 3: The linear correlation coefficient R^2 between the simulated values and theoretical values.

Materials of sphere	δ	F	p	Q_{ball}	Q_{plate}
1# elastic sphere	0.99278	0.96221	0.8174	0.85459	0.94942
2# elastic sphere	0.99864	0.97592	0.85486	0.99078	0.90207
3# elastic sphere	0.99724	0.99872	0.7483	0.99215	0.94612
4# elastic sphere	0.99714	0.99868	0.79499	0.97595	0.84714

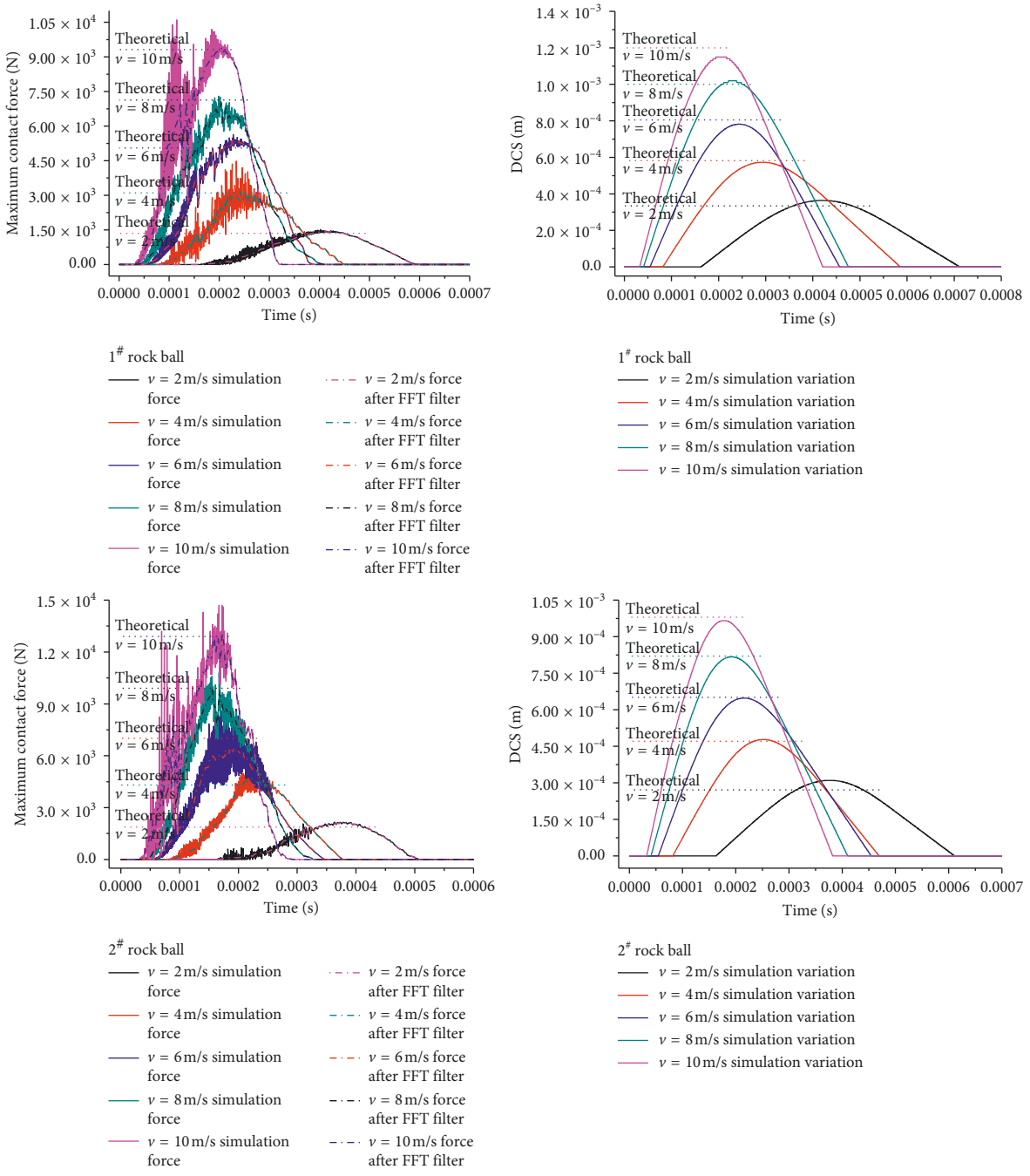

(a)

Figure 10: Continued.

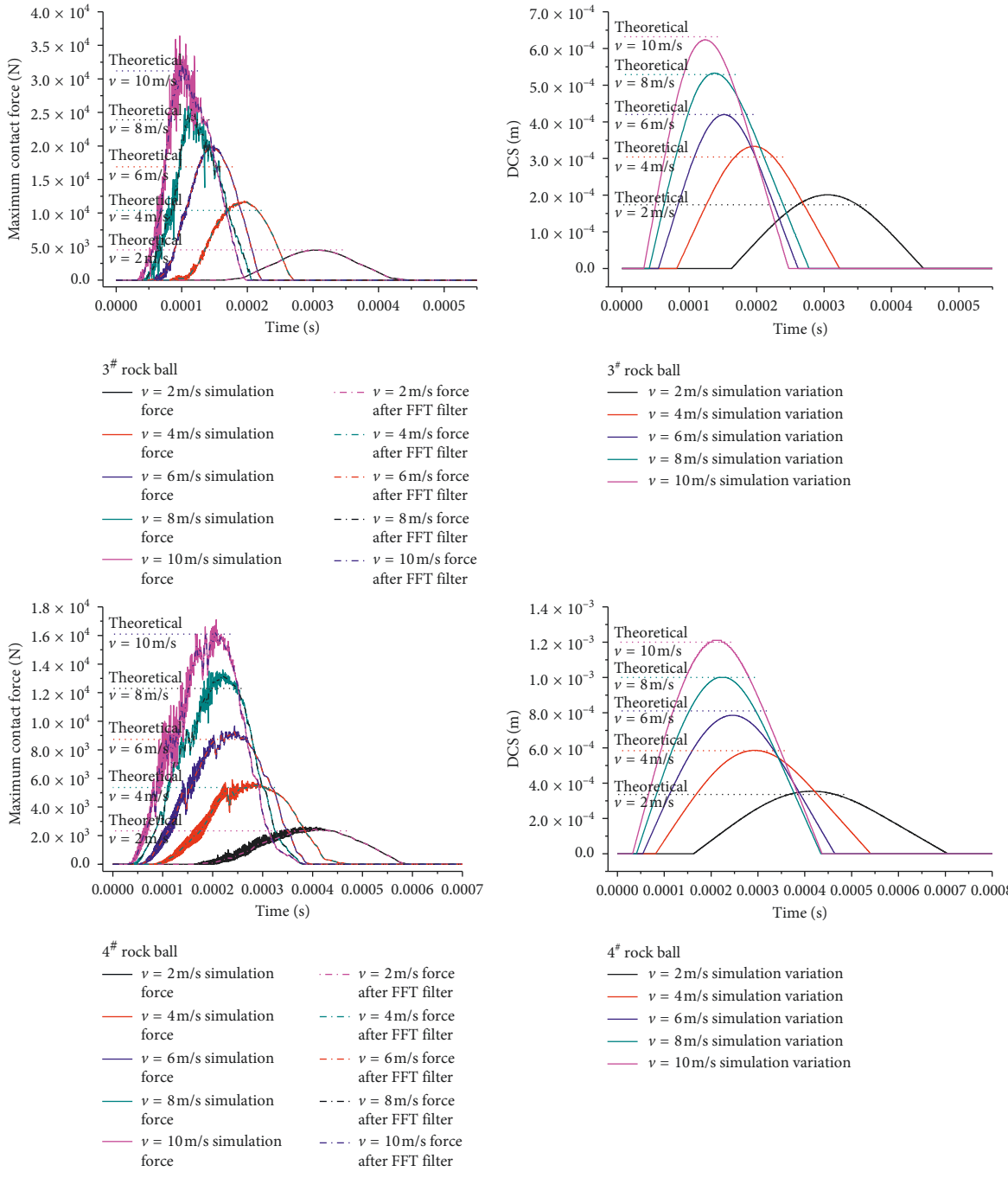

(b)

Figure 10: Force-time and DCS-time.

contact force of the sphere and DCS gradually grows with the increase of time, and then gradually decreases after reaching the peak. The reason is that when the initial kinetic energy of the sphere is converted into the energy absorbed and consumed by the sphere and the metal plate, the velocity of the sphere drops to zero, and the system enters the rebound recovery phase from the compression phase. Due to the randomness and uncertainty of the vibration, the contact force curves between the spheres and the metal plate in each group show dense vibration waves instead of smooth curves. Therefore, the method of FFT filter was used to process the simulated contact force. For different material spheres at different speeds, the theoretical values of the maximum contact force are very close with the simulation values of contact force after FFT filter, the DCS presents a smooth curve, and the simulation values of maximum DCS under various working conditions are also very close to the theoretical values. Thus, the maximum contact force and

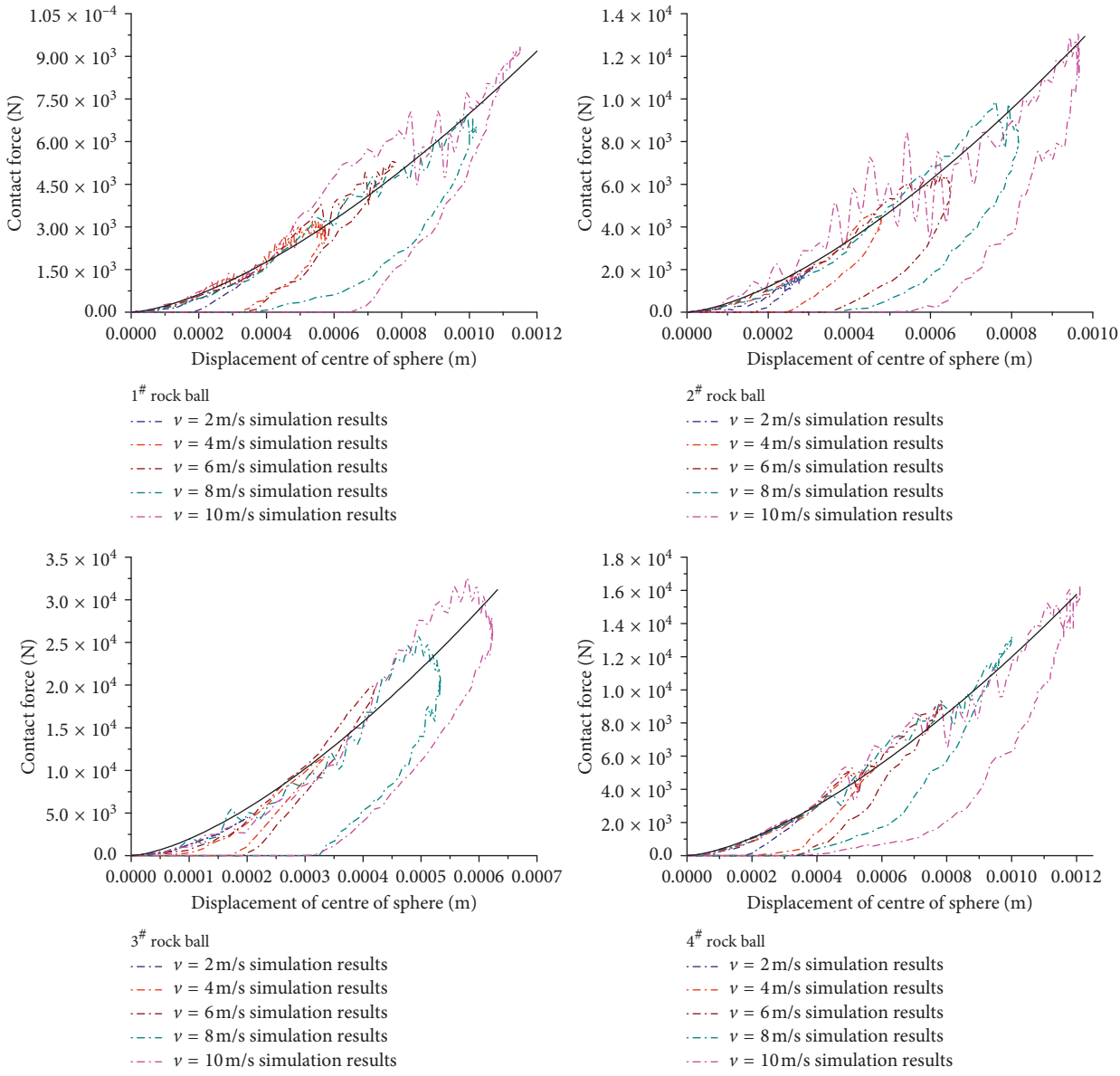

Figure 11: Force-displacement.

maximum displacement obtained by the proposed theory of the elastic sphere impacting the elastic half space in this paper are basically consistent with the corresponding results obtained by simulation.

Figure 11 shows the curves of the contact force which changes with the DCS when the four different material spheres impact the metal plate. The thick solid black lines are the theoretical curves of the compression stage, the rest are the simulation curves, and the contact force of simulation has been processed by the FFT filter. As can be seen from the figure, when the spheres with different properties impact the metal plate at different velocities, the contact force-displacement curves are all closed hysteresis loops, which is consistent with the properties revealed by the energy model considering energy absorption [32–41]. The reason for the appearing of energy hysteresis loops is the energy dissipation of the system damping, and the shapes of the contact force-displacement curves are similar to that of the experimental and simulation results [42–46]. When the sphere impacts the metal plate at five different velocities, the contact force-displacement simulation curves of the four materials fluctuate around the theoretical curves during the compression stage (before the DCS with different materials reaching its maximum values), which shows a good agreement between theoretical curves and simulation curves. The reasons for the fluctuations are as follows: (1) the randomness and uncertainty of the vibration in the process of impact contact; (2) the vibration recovery of the compressed material caused by the elasticity of the sphere and the metal plate; and (3) the calculation error of simulation software.

This paper establishes a theoretical model of an elastic sphere impacting the elastic half space. The simulation model of the viscoelastic sphere which had similar properties

with coal-gangue elastic impacting target plate in elastic half space vertically is also established. By the comparison of theory and simulation, it can be obtained that the simulation results of impact contact response have the same changing trends with the theoretical results. And the theoretical maximum contact force of the elastic sphere and theoretical maximum DCS is basically consistent with the corresponding simulation results. The theoretical models are established in this paper only considering the contact response of the sphere compression stage. The contact force-displacement simulation curves in the compression phase are in good agreement with the theoretical curves. Based on the above conclusions, the correctness of the theoretical models and the feasibility of simulation methods in the compression stage can be verified.

4. The Influence of Material Properties and Sphere Radius on the Impact Contact Response

When the elastic sphere impacts the elastic half space, the properties of the elastic sphere and the metal plate and the size of the elastic sphere have a great influence on the impact contact response of the two objects. In order to research the difference of the impact contact response caused by the change of parameters, set the variation intervals of the material properties of the elastic sphere and the metal plate (the change of properties is within the limits of different rock's properties) and set the variation interval of radius of the elastic sphere, as shown in Table 4.

From Equations (12)-(13), we obtain that

$$\delta = \frac{7}{4}\cdot\left[\frac{5\nu^2}{7}\right]^{2/5}\cdot\left[\frac{4\pi}{3}\right]^{2/5}\cdot R\cdot\rho^{2/5}\cdot\left(\frac{9}{16}\right)^{1/5}\left(\frac{1-\nu_1^2}{E_1}+\frac{1-\nu_2^2}{E_2}\right)^{2/5}, \tag{17}$$

$$P = \left(\frac{16}{9}\right)^{1/5}\left(\frac{1-\nu_1^2}{E_1}+\frac{1-\nu_2^2}{E_2}\right)^{-2/5}\left(\frac{5\nu^2}{7}\right)^{3/5}\rho^{3/5}\left(\frac{4\pi}{3}\right)^{3/5}R^2. \tag{18}$$

Hence, the DCS changes linearly with the radius R of the sphere, and the contact force is proportional to R^2, and from Table 4, $\delta/R = 0.013373106060040$, $P/R^2 = 2.161252014548062\times10^6$. The DCS and the contact force are proportional to $\rho^{2/5}$ and $\rho^{3/5}$, respectively, and $\delta/\rho^{2/5} = 1.854473633711090\times10^{-5}$, $P/\rho^{3/5} = 17.646475463447818$. The R_1 has much larger influence on DCS and maximum contact force than ρ_1.

According to the material parameters in Table 4 and Equations (17)-(18), the influence curves of the material parameters (ρ_1, E_1, ν_1) of the elastic sphere on the contact force and DCS can be obtained as shown in Figure 12. Meanwhile, the change curves of the contact force and DCS with the parameters of the metal plate material (E_2, ν_2) can be also obtained in Figure 13.

It can be seen from Figure 12, with the increase of the elastic modulus E_1, the DCS presents an exponential decrease tendency, the rate of decrease gradually reduces, and the contact force increases at a decreasing rate. The E_1 has larger influence on DCS and maximum contact force than ρ_1. With the increase of the Poisson's ratio ν_1, the DCS gradually decreases, the contact force increases gradually, and the rate of change gradually increases. The $(1-\nu_1^2)$ changes very small due to the little variations of ν_1, and the change of $(1-\nu_1^2)^{2/5}$ is smaller than $(1-\nu_1^2)$. However, the DCS and the contact force are approximately proportional to $(1-\nu_1^2)^{2/5}$ and $(1-\nu_1^2)^{-2/5}$, respectively, which leads the smallest influence of ν_1 on contact response. According to Equations (17)-(18) and Figure 12, the influence relationship of parameters on the DCS and the maximum contact force is (the sensitivity of DCS and the maximum contact force to the change of the parameter is defined as Ω) $\Omega(R) \gg \Omega(E_1) > \Omega(\rho_1) > \Omega(\nu_1)$.

Figure 13 presents that with the increase of the elastic modulus E_2 of the metal plate, the DCS shows a sharp decrease and then slows down, the maximum contact force increases quickly then slows down, and the amplitude of variation decreases gradually. With the increase of the Poisson's ratio ν_2, the DCS gradually decreases, the maximum contact force gradually increases, and the amplitude of variation gradually increases. Comparing the rangeability of the DCS and the maximum caused by the change of the metal plate's elastic modulus E_2 and by the Poisson's ratio ν_2, the rangeability of contact response caused by ν_2 is extremely small. Therefore, the influence of the metal plate parameters changes the DCS, and the maximum contact force is $\Omega(E_2) \gg \Omega(\nu_2)$.

Elastic modulus E and the Poisson's ratioν of the sphere and the metal plate both affect the results of the impact contact response. To compare the influence range of the response results caused by E_1, E_2 andν_1, ν_2, define the elastic modulus E and the Poisson's ratioν of the sphere and the metal plate with the same value and range of variation, respectively, as shown in Table 5.

Combining Equations (12)-(13), the response surface diagram of the DCS and the maximum contact force with the elastic modulus E and Poisson's ratioν can be obtained, as shown in Figure 14.

From Figure 14, it can be seen that with the increase of E_1 and E_2, the DCS and the maximum contact force decrease gradually, with the increase of ν_1 and ν_2, the DCS and the maximum contact force also gradually decrease. As shown in the figure, when E_1, E_2 or ν_1, ν_2 take the same value and change range, the resulting trend which belongs to the DCS and the maximum contact force is exactly the same, and the reason is that the relationship between the DCS/the maximum contact force and E_1 is similar to the relationship between the DCS/the maximum contact force and E_2, and the relationship between the DCS/maximum contact force and ν_1 is similar to the relationship between the DCS/the maximum contact force and ν_2, as shown in Equations (17)-(18). Therefore, if $E_1 = E_2$, $\nu_1 = \nu_2$ and $\Delta E_1 = \Delta E_2$, $\Delta\nu_1 = \Delta\nu_2$, the sensitivity of the DCS and the maximum contact force to the

Table 4: Parameters of contact model of the elastic sphere and metal plate.

Contactant		ρ_1 (kg·m^{-3})	E_1 (GPa)	ν	R (mm)
Elastic sphere	Parameters	1380	2.26	0.28	25
	Short-cut process	1000 : 60 : 3400	1 : 0.5 : 21	0.1 : 0.01 : 0.5	10 : 5 : 210
Metal plate	Parameters	7850	210	0.3	---
	Short-cut process		20 : 40 : 1620	0.1 : 0.01 : 0.5	

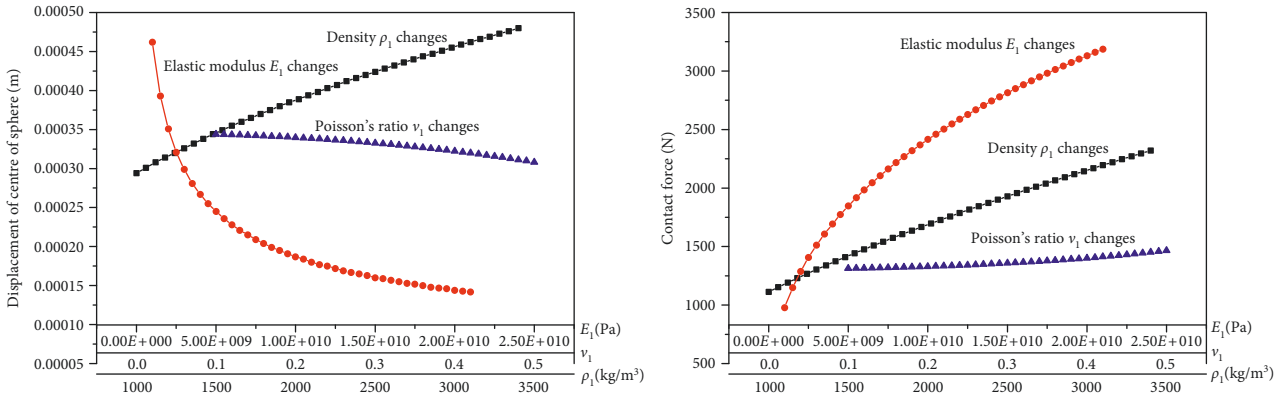

Figure 12: Effect of sphere parameters on DCS and contact force.

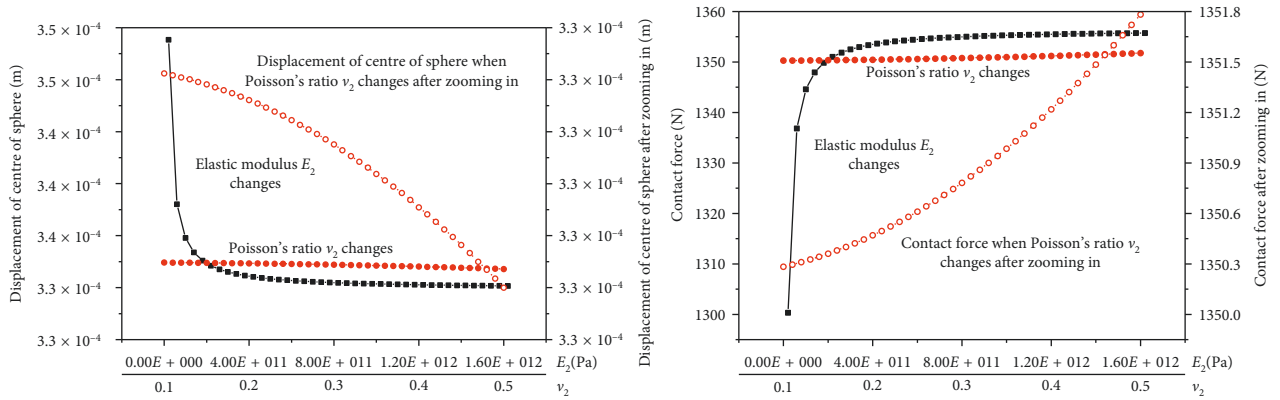

Figure 13: Effect of metal plate parameters on DCS and contact force.

Table 5: Parameters of contact model of the elastic sphere and metal plate with same properties.

Contactant		ρ_1 (kg·m^{-3})	E_1 (GPa)	ν	R (mm)
Elastic sphere	Parameters	1380	2.26	0.28	25
	Short-cut process		1 : 0.5 : 21	0.1 : 0.01 : 0.5	
Elastic plate	Parameters	1380	2.26	0.28	—
	Short-cut process		1 : 0.5 : 21	0.1 : 0.01 : 0.5	

change of parameters is $\Omega(E_1) = \Omega(E_2)$, $\Omega(\nu_1) = \Omega(\nu_2)$, i.e. $\Omega(R) \gg \Omega(E_1) = \Omega(E_2) > \Omega(\rho_1) > \Omega(\nu_1) = \Omega(\nu_2)$.

However, as for the working condition where the elastic sphere which had similar properties with rock impacting the metal plate vertically, because of the limit of intrinsic properties of the material, the E_2 is much larger than E_1 (usually at least an order of magnitude) and the values and ranges of variation of E_1 and E_2 are different. In order to study the influence of the sphere with similar properties with coal and gangue on the response of the metal plate under the two working conditions with elastic modulus E_1 and E_2, the values of E_1 and E_2 in Table 4 were taken in combination with Equations (12)-(13), and the response surface diagrams of the DCS and the maximum contact force with changes in the E_1 and E_2, respectively, are obtained, as shown in Figure 15.

In the range of values, with the increase of E_1 and E_2, the DCS presents a decreasing trend, and the maximum contact force increases. However, changing amplitude of the DCS and the maximum contact force caused by the change of the

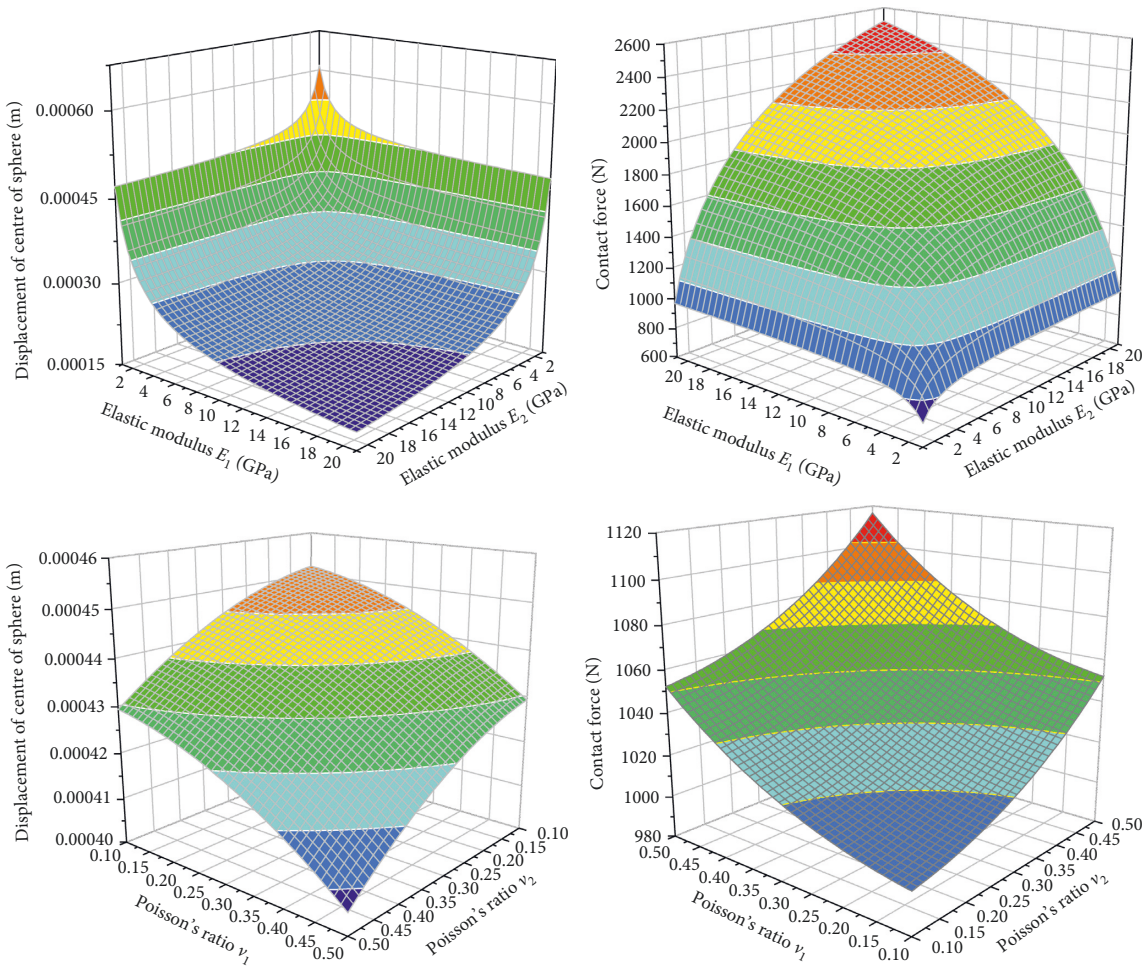

FIGURE 14: Effect of contactants' parameters on DCS and contact force in the contact process of elastic sphere impacting the elastic plate (when the elastic modulus and Poisson's ratio of the sphere are same with the plate).

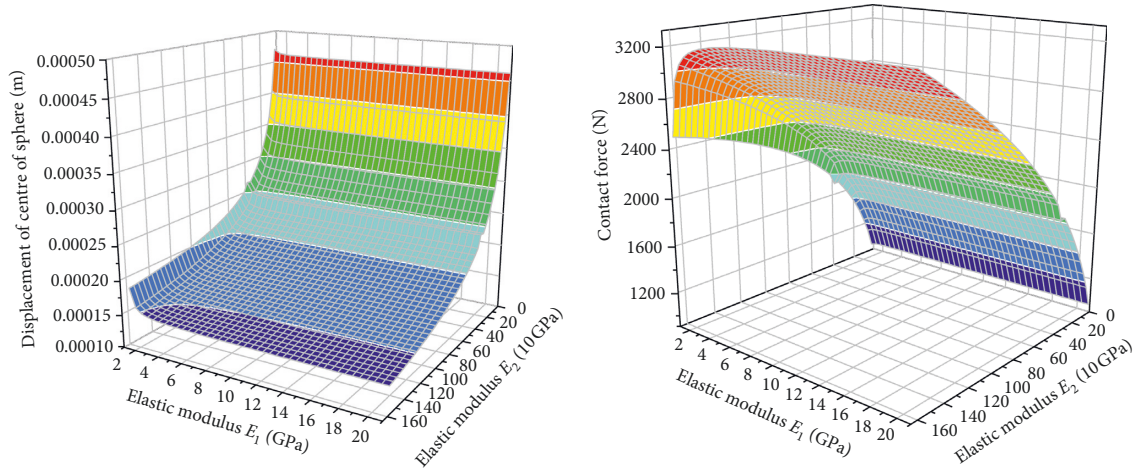

FIGURE 15: Effect of E_1 and E_2 on DCS and contact force in the contact process of elastic sphere which has similar properties with rock impacting the metal plate.

E_2 is much greater than that of the E_1. In that case, the sensitivity of the DCS and the maximum contact force to the change of the parameters is $\Omega(E_2) > \Omega(E_1)$. Meanwhile, the elastic modulus E_2 is much larger than E_1, and ν_1 is close to ν_2, which results in $(1-\mu_1^2/E_1) \gg (1-\mu_2^2/E_2)$. From Equations (17)-(18), the influence of ν_1 on the contact response is larger than the influence of ν_1 on the contact response. Therefore, $\Omega(R) \gg \Omega(E_2) > \Omega(E_1) > \Omega(\rho_1) > \Omega(\nu_1) > \Omega(\nu_2)$.

5. Case Study: Difference Analysis of Impact Contact Response of Different Materials

For the four kinds of elastic spheres with similar properties to rock as shown in Table 2, impacting the same metal plate at a speed of 10 m/s, respectively, the simulation curves of contact force-time and contact force-DCS are obtained as shown in Figures 16 and 17.

When the elastic sphere impacts the same metal plate at the same speed, the maximum contact force $P_{3\#} \gg P_{4\#} > P_{2\#} > P_{1\#}$ and the DCS $\delta_{4\#} > \delta_{1\#} > \delta_{2\#} \gg \delta_{3\#}$. Comparing the parameters of the 4 kinds of elastic spheres according to Table 2, we know $\rho_{3\#} > \rho_{4\#} \gg \rho_{2\#} > \rho_{1\#}$, $E_{3\#} \gg E_{2\#} > E_{4\#} > E_{1\#}$, $\nu_{2\#} = \nu_{3\#} \cdot > \nu_{4\#} = \nu_{1\#}$ (the definition of symbol·> is something slightly greater than something) and $R_{1\#} = R_{2\#} = R_{3\#} = R_{4\#}$; therefore, the effect of parameters R and Poisson's ratio μ can be ignored. Through the theoretical analysis of the effect of the variation of the parameters on the response results, we can get that when the elastic spheres impact the metal plate, the relationship of the sensitivity Ω of the DCS and the maximum contact force to the changing parameters is $\Omega(R) \gg \Omega(E_1) > \Omega(\rho_1) > \Omega(\nu_1)$, and the DCS will decrease and the maximum contact force will gradually increase with the increasing of elastic modulus E_1 of the elastic sphere, and the DCS and the maximum contact force are all increasing with the density ρ_1 of the elastic sphere, and the maximum contact force $P_{3\#} \gg P_{4\#} > P_{2\#} > P_{1\#}$ and the DCS $\delta_{4\#} > \delta_{1\#} > \delta_{2\#} \gg \delta_{3\#}$ can be obtained, which are same as the conclusions obtained in Figures 16 and 17.

In the four kinds of elastic spheres, $1^{\#}$ and $2^{\#}$ are elastic spheres similar to coal, and $3^{\#}$ and $4^{\#}$ are elastic spheres similar to gangue. From Figures 16 and 17, $1^{\#}$ and $2^{\#}$ elastic spheres have the obvious difference to $3^{\#}$ and $4^{\#}$ elastic spheres in the maximum contact force and DCS. Therefore, coal and gangue will cause different contact responses when impacting the metal plates in the top coal mining process, which will cause the different vibration signal of the tail beam of the hydraulic support. And the differences of impact and contact response of tail beam vibration caused by coal and gangue can be used as the basis to identify the coal-gangue.

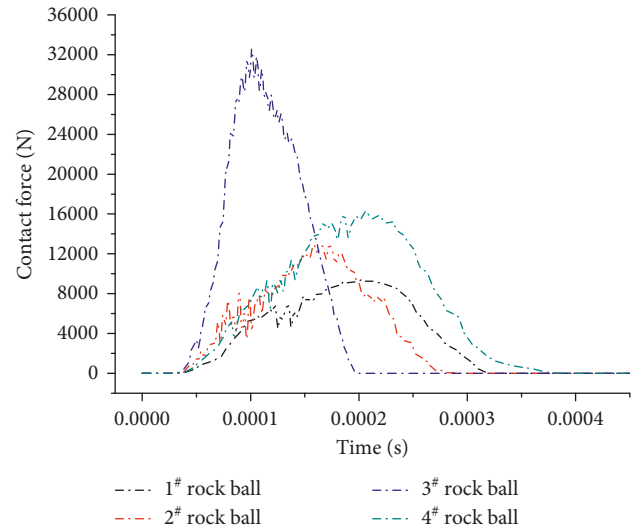

Figure 16: Simulation curves of contact force-time at 10 m/s

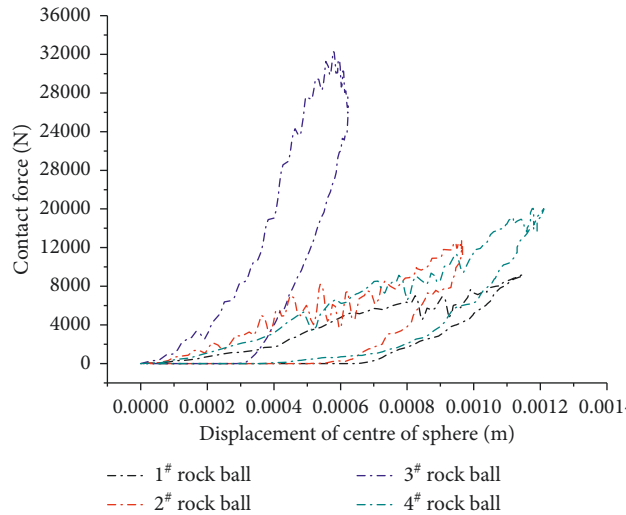

Figure 17: Simulation curves of contact force-DCS at 10 m/s.

6. Conclusion

Based on Hertz contact theory, a theoretical model of elastic sphere impacting elastic half space is established in this paper. And the finite element software LS-DYNA is used to establish a dynamic model of viscoelastic sphere impacting elastic half space, and the simulation analysis is conducted. Through the combinative and comparative analysis of theory and simulation, we obtain the following conclusions:

(1) In this paper, the contact response calculated by the theoretical model of compression stage proposed in this paper is consistent with the simulation results of the changing trend, and the maximum value and the process curve in compression stage verify the correctness of the theoretical model established in this paper and the feasibility of the simulation method in the compression stage.

(2) The theoretical model of elastic sphere impacting elastic half space proposed in this paper is more accurate to predict the maximum contact force and contact displacement. The maximum contact force calculated by the traditional contact theory is too large.

(3) The DCS and contact force are all increasing with the density ρ_1 of the elastic sphere. With the increase of elastic modulus E_1, the DCS decreases gradually and the contact force increases. With the increase of Poisson's ratio μ_1, the DCS decreases gradually and the contact force increases gradually, and the decreasing velocity of the DCS and the increasing velocity of the contact force are all increasing. With the increase of elastic modulus E_2, the DCS decreases rapidly first and then decreases slowly and the contact force increases rapidly first and then increases slowly. With the increase of Poisson's ratio

μ_2, the DCS decreases gradually and the contact force increases gradually.

(4) If the elastic sphere and plate have the same elastic modulus E and Poisson's ratio μ, influence strength (the sensitivity of DCS and the maximum contact force to the change of the parameter is defined as Ω) of the parameter of the DCS and the maximum contact force is $\Omega(R) \gg \Omega(E_1) = \Omega(E_2) > \Omega(\rho_1) > \Omega(\nu_1) = \Omega(\nu_2)$.

(5) For the condition of the elastic sphere with similar properties to rock impacting the metal plate, influence strength of the parameter on the DCS and maximum contact force is $\Omega(R) \gg \Omega(E_2) > \Omega(E_1) > \Omega(\rho_1) > \Omega(\nu_1) > \Omega(\nu_2)$.

(6) Different material properties will cause different contact response. According to the influential rule of each parameter on the response result, we can predict the difference of the results produced by the different attributes of the contact body when hitting the one target object.

The conclusions of this study will provide a theoretical basis for the accurate calculation of the contact response results, provide methods for simulation study of the impact behaviour, and provide theoretical guidance for the differences analysis of the vibration signal.

Data Availability

The data used to support the findings of this study are available from the corresponding author upon request.

Conflicts of Interest

The authors declare that there are no conflicts of interest.

Acknowledgments

This study was supported by National Natural Science Fund of China (Grant no. 51674155), Innovative Team Development Project of Ministry of Education (Grant no. IRT_16R45), Special funds for Climbing Project of Taishan Scholars, Natural Science Foundation of Shandong Province (Grant no. ZR2016EEM09), and China Postdoctoral Science Foundation (Grant no. 2016M602163).

References

[1] C. Braccesi and L. Landi, "A general elastic–plastic approach to impact analysis for stress state limit evaluation in ball screw bearings return system," *International Journal of Impact Engineering*, vol. 34, no. 7, pp. 1272–1285, 2007.

[2] R. Boettcher, A. Russell, and P. Mueller, "Energy dissipation during impacts of spheres on plates: investigation of developing elastic flexural waves," *International Journal of Solids and Structures*, vol. 106-107, pp. 229–239, 2017.

[3] V. Brizmer, Y. Kligerman, and I. Etsion, "The effect of contact conditions and material properties on the elasticity terminus of a spherical contact," *International Journal of Solids and Structures*, vol. 43, no. 18-19, pp. 5736–5749, 2006.

[4] C. Thornton, Z. M. Ning, C. Y. Wu, M. Nasrullah, and L. Y. Li, "Contact mechanics and coefficients of restitution," *Granular Gases*, vol. 564, pp. 184–194, 2001.

[5] H. Wang, X. C. Yin, X. L. Qi, Q. M. Deng, B. Yu, and Q. M. Hao, "Experimental and theoretical analysis of the elastic-plastic normal repeated impacts of a sphere on a beam," *International Journal of Solids and Structures*, vol. 109, pp. 131–142, 2017.

[6] L. Kogut and I. Etsion, "Elastic–plastic contact analysis of a sphere and a rigid flat," *Journal of Applied Mechanics*, vol. 69, no. 5, pp. 657–662, 2002.

[7] K. T. Chau, R. H. C. Wong, and J. J. Wu, "Coefficient of restitution and rotational motions of rockfall impacts," *International Journal of Rock Mechanics and Mining Sciences*, vol. 39, no. 1, pp. 69–77, 2002.

[8] O. Cermik, H. Ghaednia, and D. B. Marghitu, "Analytical study of the oblique impact of an elastic sphere with a rigid flat," in *Proceedings of Acoustics and Vibration of Mechanical Structures Conference*, Timisoara, Romania, May 2018.

[9] Y. A. Rossikhin, M. V. Shitikova, and M. S. Khalid, "Impact-induced internal resonance phenomena in nonlinear doubly curved shallow shells with rectangular base. Analysis and Modelling of Advanced Structures and Smart Systems," in *Advanced Structured Materials*, vol. 81, pp. 149–189, 2018.

[10] J. Xi, M. Dong, S. F. Li, Y. Shang, and Z. Fu, "Dynamic characteristics for the normal impact process of microparticles with a flat surface," *Aerosol Science and Technology*, vol. 52, no. 2, 2017.

[11] E. Willert, I. A. Lyashenko, and V. L. Popov, "Influence of the Tabor parameter on the adhesive normal impact of spheres in Maugis-Dugdale approximation," *Computational Particle Mechanics*, vol. 5, no. 3, pp. 313–318, 2017.

[12] W. J. Stronge and A. D. C. Ashcroft, "Oblique impact of inflated balls at large deflections," *International Journal of Impact Engineering*, vol. 34, no. 6, pp. 1003–1019, 2007.

[13] C. Thornton, S. J. Cummins, and P. W. Cleary, "On elastic-plastic normal contact force models, with and without adhesion," *Powder Technology*, vol. 315, pp. 339–346, 2017.

[14] H. F. Xiao, M. J. Brennan, and Y. M. Shao, "On the undamped free vibration of a mass interacting with a Hertzian contact stiffness," *Mechanics Research Communications*, vol. 38, no. 8, pp. 560–564, 2011.

[15] T. J. Wang, L. Q. Wang, L. Gu, and D. Z. Zheng, "Stress analysis of elastic coated solids in point contact," *Tribology International*, vol. 86, pp. 52–61, 2015.

[16] Z. J. Wang, H. Yu, and Q. Wang, "Layer-substrate system with an imperfectly bonded interface: spring-like condition," *International Journal of Mechanical Sciences*, vol. 134, pp. 315–335, 2017.

[17] E. Willert, S. Kusche, and V. L. Popov, "The influence of viscoelasticity on velocitydependent restitutions in the oblique impact of spheres," *Facta Universitatis, Series: Mechanical Engineering*, vol. 15, no. 2, pp. 269–284, 2017.

[18] J. P. Mougin, P. Perrotin, M. Mommessin, J. Tonnelob, and A. Agbossou, "Rock fall impact on reinforced concrete slab: an experimental approach," *International Journal of Impact Engineering*, vol. 31, no. 2, pp. 169–183, 2005.

[19] J. Jäger, "Properties of equal bodies in contact with friction," *International Journal of Solids and Structures*, vol. 40, no. 19, pp. 5051–5061, 2003.

[20] C. Y. Wu, L. Y. Li, and C. Thornton, "Rebound behaviour of spheres for plastic impacts," *International Journal of Impact Engineering*, vol. 28, no. 9, pp. 929–946, 2003.

[21] C. S. Liu, K. Zhang, and R. Yang, "The FEM analysis and approximate model for cylindrical joints with clearances," *Mechanism and Machine Theory*, vol. 42, no. 2, pp. 183–197, 2007.

[22] L. Vu-Quoc, L. Lesburg, and X. Zhang, "An accurate tangential force–displacement model for granular-flow simulations: contacting spheres with plastic deformation, force-driven formulation," *Journal of Computational Physics*, vol. 196, no. 1, pp. 298–326, 2004.

[23] L. Vu-Quoc, X. Zhang, and L. Lesburg, "Normal and tangential force–displacement relations for frictional elasto-plastic contact of spheres," *International Journal of Solids and Structures*, vol. 38, pp. 6455–6489, 2001.

[24] J. Y. Wang, Z. Y. Liu, and J. Z. Hong, "Influence of non-physical chosen parameters on impact dynamics of discretized elastic bodies," *Journal of Mechanics*, pp. 1–11, 2017.

[25] P. Peng, C. Di, L. Qian, and G. Chen, "Parameter identification and experimental investigation of sphere-plane contact impact dynamics," *Experimental Techniques*, vol. 41, no. 5, pp. 547–555, 2017.

[26] T. M. Pham, Y. F. Hao, and H. Hao, "Sensitivity of impact behaviour of RC beams to contact stiffness," *International Journal of Impact Engineering*, vol. 112, pp. 155–164, 2018.

[27] X. D. Chen and A. H. C. Chan, "Modelling impact fracture and fragmentation of laminated glass using the combined finite-discrete element method," *International Journal of Impact Engineering*, vol. 112, pp. 15–29, 2018.

[28] J. F. Liu, Y. Long, C. Jia, Q. Liu, M. S. Zhong, and Y. Zhou, "Influence of layer number and air gap on the ballistic performance of multi-layered targets subjected to high velocity impact by copper EFP," *International Journal of Impact Engineering*, vol. 112, pp. 52–65, 2018.

[29] X. Q. Cheng, J. Zhang, J. W. Bao, B. Y. Zeng, Y. J. Cheng, and R. W. Hu, "Low-velocity impact performance and effect factor analysis of scarf-repaired composite laminates," *International Journal of Impact Engineering*, vol. 111, pp. 85–93, 2017.

[30] K. L. Johnson, *Contact Mechanics*, Cambridge University Press, Cambridge, UK, 1985.

[31] S. M. He, J. Shen, Y. Luo, and Y. Wu, "Study on the characteristics of normal impact of post-earthquake rock-fall on slope," *Engineering Mechanics*, vol. 28, no. 6, pp. 118–124, 2011.

[32] K. Hunt and E. Crossley, "Coefficient of restitution interpreted as damping in vibroimpact," *Journal of Applied Mechanics*, vol. 42, no. 2, pp. 440–445, 1975.

[33] R. G. Herbert and D. C. McWhannell, "Shape and frequency composition of pulses from an impact pair," *Journal of Engineering for Industry*, vol. 99, no. 3, pp. 663–671, 1977.

[34] H. M. Lankarani and P. E. Nikravesh, "A contact force model with hysteresis damping for impact analysis of multibody systems," *Journal of Mechanical Design*, vol. 112, no. 3, pp. 369–376, 1990.

[35] H. M. Lankarani and P. E. Nikravesh, "Continuous contact force models for impact analysis in multibody systems," *Nonlinear Dynamics*, vol. 5, no. 2, pp. 193–207, 1994.

[36] Y. Gonthier, J. Mcphee, C. Lange, and J. C. Piedbœuf, "A regularized contact model with asymmetric damping and dwell-time dependent friction," *Multibody System Dynamics*, vol. 11, no. 3, pp. 209–233, 2004.

[37] M. Machado, P. Moreira, P. Flores, and H. M. Lankarani, "Compliant contact force models in multibody dynamics: evolution of the Hertz contact theory," *Mechanism and Machine Theory*, vol. 53, pp. 99–121, 2012.

[38] P. Flores, M. Machado, M. T. Silva, and J. Martins, "On the continuous contact force models for soft materials in multibody dynamics," *Multibody System Dynamics*, vol. 25, no. 3, pp. 357–375, 2011.

[39] P. Flores, J. Ambrósio, J. C. P. Claro, and H. M. Lankarani, "Dynamic behaviour of planar rigid multi-body systems including revolute joints with clearance," *Proceedings of the Institution of Mechanical Engineers, Part K: Journal of Multibody Dynamics*, vol. 221, no. 2, pp. 161–174, 2015.

[40] P. Flores, C. S. Koshy, H. M. Lankarani, J. Ambrósio, and J. C. P. Claro, "Numerical and experimental investigation on multibody systems with revolute clearance joints," *Nonlinear Dynamics*, vol. 65, no. 4, pp. 383–398, 2011.

[41] P. Flores, "A parametric study on the dynamic response of planar multibody systems with multiple clearance joints," *Nonlinear Dynamics*, vol. 61, pp. 633–653, 2010.

[42] Y. Chen, "Research on characteristics of damage behavior and dynamic response of fibre-metal laminateunder impact load," M.S. thesis, Harbin Institute of Technology, Harbin, China, 2014.

[43] X. P. Zeng, "Analysis of damage properties in glass fiber reinforced aluminum alloy laminates under low velocity impact," M.S. thesis, Harbin Institute of Technology, Harbin, China, 2012.

[44] H. W. Hu, "Study of experimental and numerical analysis method of FMLs subjected to low velocity impact," M.S. thesis, Northwestern Polytechnical University, Xi'an, China, 2015.

[45] X. Liu, "The research on dynamic response and low-energy impact damage of composite laminated structures in aircraft," M.S. thesis, South China University of Technology, Guangzhou, China, 2012.

[46] F. N. Tan, "Mechanical properties of foam sandwich composites with low-velocity impact damage," M.S. thesis, Shanghai Jiao Tong University, Shanghai, China, 2012.